Dynamics of Protein and Chromophore Structural Changes in the Photocycle of Photoactive Yellow Protein Monitored by Time-Resolved Optical Rotatory Dispersion[†,‡]

Eefei Chen,[§,||] Thomas Gensch,[||,⊥,@] Andrew B. Gross,[§] Johnny Hendriks,[⊥] Klaas J. Hellingwerf,[⊥] and David S. Kliger*[,§]

Department of Chemistry and Biochemistry, University of California, Santa Cruz, California 95064, and Laboratory for Microbiology, Swammerdam Institute of Life Science, Nieuwe Achtergracht, 166, 1018 WV Amsterdam, The Netherlands

Received September 9, 2002; Revised Manuscript Received December 13, 2002

ABSTRACT: The dynamics of the PYP photocycle have been studied using time-resolved optical rotatory dispersion (TRORD) spectroscopy in the visible and far-UV spectral regions to probe the changes in the chromophore configuration and the protein secondary structure, respectively. The changes in the secondary structure in PYP upon photoisomerization of the chromophore can be described by two exponential lifetimes of 2 ± 0.8 and 650 ± 100 ms that correspond to unfolding and refolding processes, respectively. The TRORD experiments that follow the dynamics of the chromophore report three exponential components, with lifetimes of 10 ± 3 μs, 1.5 ± 0.5 ms, and 515 ± 110 ms. A comparison of the kinetic behaviors of the chromophore and protein shows that during the decay of pR_{465} an initial relaxation that is localized to the chromophore hydrophobic pocket precedes the formation of the chromophore and protein structures found in pB_{355}. In contrast, the protein and chromophore processes occur with similar time constants during inactivation of the signaling state.

Light receptors which act as photosensory transducers in living organisms monitor spectral and intensity changes in environmental light conditions and initiate an appropriate behavioral response. For example, the plant photoreceptor phytochrome plays a regulatory role, based on its sensitivity to environmental far-red and red light, in photomorphogenetic processes such as flowering, seed germination, and chlorophyll synthesis. In halobacteria, sensory rhodopsins modulate the direction of rotation of the cell's flagellar motor in response to light intensity and color, thus leading to a process that is loosely termed phototaxis. In the phototropic bacterium *Ectothiorhodospira halophila*, a negative phototactic response appears to be mediated by the blue light photoreceptor photoactive yellow protein (PYP)[1] (*1*). Because PYP is a relatively small cytosolic protein that is accessible for high-resolution X-ray diffraction and NMR structure determinations, it serves as a model system for understanding light-triggered signal transduction.

PYP consists of 125 amino acids (14 kDa) with a *p*-coumaric acid (4-hydroxycinnamyl) chromophore covalently linked through a thioester bond to Cys69 (*2*−*5*). Although the *p*-coumaric chromophore in PYP is distinctly different from the retinal chromophore found in rhodopsins, some photophysical and photochemical properties of PYP are notably similar to those of sensory rhodopsin. The mechanism of signal transduction in sensory rhodopsin, PYP, and phytochrome depends on an initially small configurational change of the chromophore that leads to protein conformational changes, which results in the alteration of protein−protein interactions and finally in a behavioral response. The protein conformational changes are triggered by a *trans*−*cis* chromophore isomerization (*6*−*11*), which most probably occurs on a picosecond time scale.

The chromophore-localized primary event of the PYP photocycle has been probed with steady state low-temperature visible and infrared absorption (*10*, *12*, *13*), femtosecond to nanosecond transient UV−vis absorption (*11*, *14*−*17*), and fluorescence studies (*18*−*20*). Excellent structural characterization of the ground (dark) state, pG_{446}, is available from X-ray diffraction (*21*, *22*) and solution NMR (*23*) studies. In addition, high-resolution diffraction data have been measured for the red-shifted pR_{465} intermediate [1.9 (*7*) and 1.8 Å (*9*) resolution, respectively], a pre-pR_{465} cryotrapped intermediate (PYP_{BL}) (*8*), and the blue-shifted state, pB_{355} (*24*). Although there are still significant differences in the

[†] This research was funded in part by National Institute of General Medical Sciences (NIH) Grant GM38549 (D.S.K.), the Netherlands Foundation for Chemical Research with financial assistance from the Netherlands Organization for Scientific Research (K.J.H. and J.H.), and the Royal Dutch Academy of Science and the Nordrhein-Westfälische Akademie der Wissenschaften through a Casimir-Ziegler fellowship (T.G.).

[‡] We dedicate this paper to Professor Silvia Braslavsky on the occasion of her 60th birthday.

* To whom correspondence should be addressed. E-mail: kliger@chemistry.ucsc.edu.

[§] University of California.

[||] Both authors contributed equally to this work.

[⊥] Swammerdam Institute of Life Science.

[@] Present address: Institute of Biologal Information Processing 1-Cellular Processes, Research Centre Jülich, D-52425 Jülich, Germany.

[1] Abbreviations: PYP, photoactive yellow protein; TRORD, time-resolved optical rotatory dispersion; TRCD, time-resolved circular dichroism; TROD, time-resolved UV−vis absorption; ORD, optical rotatory dispersion; CD, circular dichroism; OMA, optical multichannel analyzer; SVD, singular-value decomposition.

10.1021/bi020577o CCC: $25.00
Published on Web 01/30/2003

interpretation of the results obtained by application of these various techniques, some widely accepted features have emerged.[2]

There are up to four precursors to the pR_{465} intermediate, which forms within a few nanoseconds (*15*). The most prominent of these is detected within a few picoseconds in transient absorption studies (alternatively termed I_0 or PYP_B) and is characterized by an absorption maximum (~500 nm) that is red-shifted from that of pG_{446} (*15*, *16*). Recent femtosecond anisotropy measurements have shown that in the I_0 state the photoisomerization has already occurred (*11*), while a number of subsequent relaxation steps of the chromophore and the neighboring amino acids occur during pR_{465} formation. pR_{465} decays multiexponentially within milliseconds to the putative signaling state pB_{355} (*27*−*29*). Formation of pB_{355} is accompanied by several structural events, including protonation of the chromophore and protein conformational changes, and is best described by two highly temperature and pH dependent exponential terms, 250 μs and 1.2 ms (19 °C, pH 7.5) (*28*). Assignment of the observed proton uptake during the PYP photocycle (*30*) to chromophore protonation by Glu46 during the formation of pB_{355} has been reported by several FTIR studies (*26*, *31*, *32*). Although measurements of light-dependent pH changes in wild-type PYP and two variants (H108F and E46Q) using transient absorption methods also support proton donation to the chromophore by Glu46 at slightly alkaline pH (7.5−8.5), the possibility of proton transfer from the solvent could not be ruled out (*33*). This is also offered as a possible alternative interpretation in the time-resolved FTIR studies by Brudler et al. (*34*). In fact, the results of a time-resolved absorption study of pB_{355} using pH-indicator dyes with wild-type PYP and E46Q and E46A variants suggest that the chromophore can directly be protonated by the solvent (*35*). The decay of pB_{355} back to pG_{446} occurs on a subsecond to seconds time scale and is also described by two exponential processes, 150 ms and 2 s.

The pR_{465} intermediate is proposed to have a fully *cis* chromophore configuration, while maintaining a global protein structure similar to that of pG_{446}. From FT Raman and step scan FTIR spectroscopic studies, formation of a pR′ (I_1′) intermediate (τ = 113 μs) was associated with movement of the protonated Glu46 into a hydrophobic environment and protonation of the chromophore phenolic group in ~25% of the PYP molecules (*34*). The formation of pR′ from pR_{465} was described in parallel with deprotonation of Glu46 to form pB_{355} in the remaining 75% PYP molecules. An additional intermediate (I_2′) was proposed by Brudler et al. (*34*) but reportedly follows pB_{355} (I_2) too closely in time to allow definition of specific differences between them. However, a state of PYP with a protonated chromophore (τ = 250 μs) was identified with time-resolved FTIR spectroscopy (*26*) and was suggested to be formed by proton transfer from Glu46 to the chromophore (*31*, *32*). Because this latter transition was not accompanied by significant differences in the global protein structure, this state was assigned as an intermediate (pB′) distinct from and preceding the pB_{355} species, but with the same absorption maximum. Large conformational changes have been observed on the time scale of 2 ms for the pB′ → pB_{355} transition. These conformational changes can be observed in solution and in well-hydrated films, but not in crystals or in dry films (*25*, *26*), which helps to explain the results of X-ray crystallography studies that show no large protein conformational changes throughout the PYP photocycle. According to these FTIR studies, the charged Glu46 in pB′ that is buried in an energetically unfavorable, highly hydrophobic cavity may trigger the large global conformational changes that accompany the formation of pB_{355}.

The global conformational changes that are involved in the formation of pB_{355} are likely to be instrumental in the mechanism of the negative phototactic response triggered by PYP (*25*, *26*, *29*, *34*−*39*). Solvent hydrophobicity and viscosity studies have suggested that during the photocycle the protein conformation changes, to temporarily expose a hydrophobic patch to the solvent (*29*, *37*). In a recent study with a polarity sensitive fluorescent probe, it was found that pB_{355} formation is accompanied by the exposure of a hydrophobic surface on a time scale that is 8 times slower than protonation of the chromophore (*38*). This is supported by an absorption study that suggests bromocresol purple binds with a time constant of 3.2 ms to the hydrophobic surface that is exposed during formation of pB_{355} (*35*). These results are consistent with time-resolved FTIR studies that report chromophore protonation at ~250 μs and protein conformational changes at ~2 ms (*26*, *34*). Because it was shown that such an increase in hydrophobicity facilitates binding of PYP to lipid bilayers (*36*) and because pB_{355} is the only intermediate with a lifetime that is sufficiently long to transmit the information of blue light absorption to a signal transduction partner protein, pB_{355} is believed to be the biologically significant "activated" signal transduction state. Partial unfolding of the protein is proposed to accompany formation of the signaling state, whereas protein refolding facilitates the return of the chromophore to the *trans* configuration of the pG_{446} (*29*). Chromophore-triggered protein conformational changes as a mechanism for activation of signaling state formation have previously been proposed for the sensory rhodopsin I and II photoreceptors (*40*) and the phytochrome plant photoreceptor (*41*). For PYP too, several lines of evidence for such a mechanism have been found, in the results of fluorescence and FTIR studies (*26*, *38*). However, Brudler et al. have interpreted the FTIR dynamics of the PYP photocycle along the lines of a parallel kinetic mechanism, where the chromophore, protonation, and protein backbone events (τ = 113 μs and 1.5 ms) occur synchronously (*34*).

We have studied PYP with time-resolved optical rotatory dispersion (TRORD) spectroscopy in the far-UV and visible regions to probe the changes in the protein secondary structure and in the chromophore, respectively, throughout the photocycle. TRORD, rather than time-resolved circular dichroism (TRCD), spectroscopy is used to follow the

[2] A review of the literature shows that the PYP photocycle intermediates have been identified by different nomenclatures. For example, pR_{465} and pB_{355} are also known as I_1 or PYP_L and I_2 or PYP_M, respectively. Because new intermediates, which cannot be observed by absorption techniques, have been identified with vibrational, photoacoustic, and photothermal methods (*25*, *26*; T. Gensch, A. Losi, J. Hendriks, K. J. Hellingwerf, and S. E. Braslavsky, unpublished results; M. Terazima, personal communication), a unified and systematic nomenclature would be beneficial. However, until one is available we will use pR_{465} to describe the red-shifted intermediate, pB_{355} to describe the blue-shifted state, and pG_{446} to describe the dark state (or initial state) species.

kinetics of the PYP photocycle because optical rotatory dispersion (ORD) detection provides a signal-to-noise advantage over circular dichroism (CD) measurements. However, because CD spectra are more sensitive to secondary structure differences, equilibrium CD measurements are used to provide a structural interpretation of the ORD data. To demonstrate that our experimental conditions and results are comparable to those of previous spectroscopic studies, we have also performed time-resolved UV−vis absorption (TROD) experiments.

The results of these studies provide insight into the protein−chromophore interactions at each stage of the photocycle from microseconds to seconds. The changes in the secondary structure in PYP upon photoisomerization can be described by two exponential lifetimes of 2 ± 0.8 and 650 ± 100 ms that correspond to unfolding and refolding processes, respectively. Analysis of equilibrium CD spectra suggests that the secondary structure changes during formation of pB_{355} are attributed largely to unfolding of α-helical protein structure. The TRORD experiments that follow the dynamics of the chromophore report three exponential components, with lifetimes of 10 ± 3 μs, 1.5 ± 0.5 ms, and 515 ± 110 ms. The photocycle mechanism can be described by changes in the geometry of the chromophore that precede and facilitate the formation of the signaling state, whereas the structural changes in the chromophore and protein occur with the same time constant during re-formation of pG_{446}.

MATERIALS AND METHODS

Sample Preparation. Recombinant apoPYP was produced heterologously in *Escherichia coli*, as described previously (*42*). ApoPYP was reconstituted with a carbonyl diimidazole (CDI) derivative of *p*-coumaric acid (pCA) (adapted from refs *43* and *44*). The derivative was prepared by dissolving equal amounts of pCA and CDI to a final concentration of 250 mM in dry *N*,*N*′-dimethylformamide and stirring it overnight at 4 °C. The PYP sample was used after cleavage and removal of its polyhistidine tail.

For TRORD experiments, PYP samples (90 μM) were prepared by dilution of a concentrated PYP stock solution into 5 mM TRIS buffer (pH 8). This solution has an absorbance of ∼1 in a 1.3 mm cell at 230 nm and an absorbance of ∼0.8 in a 2 mm cell at 446 nm for the TRORD experiments, and an absorbance of ∼0.5 in a 1.3 mm cell at 446 nm for TROD experiments.

For equilibrium CD and ORD measurements, PYP samples (∼20 μM) were prepared by dilution of the concentrated PYP stock solution into deionized (DI) water. DI water, rather than 5 mM TRIS buffer, was used so that data near 180 nm could be measured. The pH of the DI water was adjusted with 1 M HCl or 1 M NaOH to yield sample pH values of 8, 6, 4, 3, and 1.5. In this study, the form of PYP at pH 1.5 is termed the pB_{dark} species.

Equilibrium ORD signals were collected for pB_{dark} and for pB_{355} that was obtained by continuous illumination of PYP at pH 4 with a 12 V, 50 W tungsten halogen lamp (HLX 64 610 BRL, Osram) and a 450 nm cutoff filter. The steady state absorption spectra of PYP were measured on a UV−vis spectrophotometer (UV-2101PC, Shimadzu, Columbia, MD), and PYP concentrations were calculated by using an ϵ_{446} of 45 500 M^{-1} cm^{-1} (*29*, *45*).

Time-Resolved Optical Rotatory Dispersion and Absorption Systems. The PYP photocycle was initiated with 0.4−0.6 mJ, 7 ns pulse width (full width at half-maximum) light of 444 nm generated by a Quanta-Ray PDL-1 dye laser that was pumped by the third harmonic of a Quanta-Ray DCR-1 Nd:YAG laser (Spectra-Physics, Mountain View, CA). Spectral changes induced by laser excitation were probed with a xenon flash lamp. The TRORD technique has been described by Shapiro et al. (*46*). Briefly, the sample cell was positioned between two MgF_2 polarizers oriented at 90° (crossed position) relative to each other. The initially unpolarized probe light was first collimated with a fused silica lens before it passed through the first polarizer, the sample, and then the second, analyzing polarizer. In these experiments, the first polarizer was rotated by $\pm\beta$ (1.87°) from the crossed position. The probe beam was focused onto the slit of a spectrograph before it was dispersed by a grating (600 g/mm) that is blazed at 200 nm and detected by an optical multichannel analyzer (OMA) detector.

Recent modifications of the TRORD system, where mirrors are used to focus the probe beam down to a spot with a diameter of ∼300 μm, have allowed the use of considerably smaller sample volumes. The pump beam was focused down to ∼2 mm in diameter and was overlapped with the probe beam at the sample cell, entering ∼15° relative to the probe light. The propagation axis of the probe beam was perpendicular to the face of the sample. Modifications of the original TRORD design to permit experiments on these small sample volumes will be described elsewhere.

For TROD experiments, the TRORD configuration was modified by removing the polarizers. The details of the TROD system have been described previously (*47*).

Time-Resolved Measurements. The sample was recycled with a peristaltic pump between the flow cell, which was made with fused silica windows, and a sample reservoir. Data were collected with a 2 s delay between each laser pulse so that the irradiated sample could flow out of the pump−probe path before the next laser flash would arrive. This precaution was taken to avoid the buildup of photodegradation products or long-lived photoproducts that could interfere with the kinetics of the photocycle. Care was also taken to detect significant fluctuations in temperature, laser power, and pump−probe geometry. The temperature of the sample (24−26 °C) and the laser power were measured several times throughout the experiment with an infrared temperature probe (Fluke 80T-IR, Fluke Corp., Everett, WA) and an Ophir power meter (Ophir-Aryt Optronics, Ltd., Jerusalem, Israel), respectively. An absorption spectrum was measured periodically throughout the experiments to ensure the integrity of the photoreceptor protein.

For TRORD experiments in the far-UV region, approximately 300 averages at each of 20 delay times between 50 μs and 2.1 s were collected after photoinitiation. In the visible region (430−530 nm), 19 time points were measured between 500 ns and 800 ms after initiation of the photocycle. At 500 ns and 1 μs, ∼1000 averages were recorded, while ∼594 averages were accumulated at all other times. The TROD spectra were often collected on the same sample used for the far-UV TRORD experiments. For each set of TROD data, two averages were collected at two to six logarithmic delay times per decade between 1 μs and 2 s after the photocycle was initiated. The data shown in this paper

represent a total of 16 averages for each of the 30 time points that were measured. The time resolution of the far-UV and visible TRORD experiments was 50 μs and 500 ns, respectively, whereas the time resolution for the TROD experiments was 1 μs.

Circular Dichroism Measurements. CD spectra of PYP at different pH values were measured on an AVIV 60DS spectrometer (AVIV Associates, Lakewood, NJ). Data were accumulated for 16 s every 1 nm with a bandwidth of 1 nm from 180 to 280 nm using a 1 mm quartz cuvette. The temperature in all experiments was maintained between 24 and 26 °C.

SVD and Global Analysis. The time-dependent behavior of the TRORD and TROD data in both spectral regions was analyzed using singular-value decomposition (SVD) and global exponential fitting algorithms, which were written in the mathematical software package Matlab (Pro-Matlab, The Mathworks Inc., South Natick, MA). Two studies on the plant photoreceptor phytochrome (*47*, *48*) give details of SVD and global analysis methods, so they are not discussed here.

The OMA TRORD data from the visible and far-UV spectral regions were analyzed in the form of difference ORD signals, obtained by subtracting the initial state PYP ORD signal from the signal of PYP measured at various time points after initiation of the photocycle. The OMA far-UV TRORD data in the 210−260 nm spectral range, as well as several data sets that were truncated around 230 nm, were analyzed. The far-UV and visible TRORD spectra were also analyzed as single-wavelength difference TRORD data because the photoinduced changes are small. The kinetic traces for the far-UV and visible TRORD data were obtained by averaging the difference OMA data across the 228−232 and 468−472 nm wavelength regions at each time point. Consequently, the exponential lifetimes reported in the Results for the far-UV and visible TRORD data are averages of the values reported separately by analysis of the OMA and kinetic data. The far-UV TRORD data were offset near 270 nm because the equilibrium OR spectra of pG_{446}, pB_{dark}, and pB_{355} showed no optical activity from 265 to 270 nm and weak optical activity from 275 to 300 nm.

The TRORD data obtained in the visible region showed unusual structure at wavelengths greater than 500 nm, well to the red of the wavelength maximum (460 nm) of the pG_{446} ORD signal. It was later determined that these features were caused by second-order diffraction from the spectrograph grating. To correct for this artifact, equilibrium ORD signals for pG_{446} were measured with and without a 320 nm cutoff filter (O-54, Corning Glass Works, Corning, NY). The difference signal of pG_{446} without and with the filter was used to correct the TRORD signals. Cutoff filter measurements for pB_{355} and pB_{dark} yielded similar baseline corrections.

The OMA TROD data were also analyzed as difference spectra of PYP measured at various time delays after initiation of the photocycle minus PYP measured before photoinitiation. The TROD spectra were only analyzed in the form of OMA data. However, the TROD data are also presented as a kinetic trace by averaging the OMA data from 444 to 448 nm for comparison with the TRORD data.

CD Spectral Analysis. The contributions of various elements of secondary structure to the equilibrium CD spectra of PYP at different pH values were analyzed using the CDsstr program described by Johnson (*49*). CDsstr implements an SVD algorithm that combines the ideas of many previous workers to estimate the secondary structure of proteins and uses the CD spectra of proteins with known structures as the basis set. The CDsstr method gives a root-mean-square error of 4% or better for the secondary structures of an α-helix, 3_{10}-helix, β-strand, turn, and poly(L-proline) II type 3_1-helix for the proteins in the basis set. This error is of approximately the same size as the uncertainty in the secondary structure determination that was reported with X-ray diffraction for these proteins. The input files included PYP and myoglobin CD data in the wavelength region of ~181−260 nm. The myoglobin data were provided as test data by the CDsstr web site (randymacdonald.als.orst.edu) and were used to confirm that the CDsstr program was running according to specifications. Twenty-six protein spectra were used as a basis set, and the resulting fits of PYP were compared to the results of X-ray (*21*) and NMR (*23*) structure determinations.

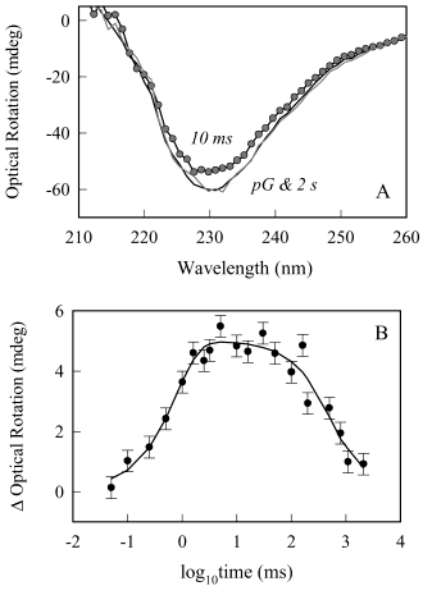

FIGURE 1: Far-UV TRORD data on the kinetics of the PYP photocycle. The pG_{446} ORD signal (black line) and the ORD signals measured 10 ms (gray circles) and 2 s (gray line) after initiation of the photocycle are shown in panel A. The difference ORD intensities (230 nm) measured at all time points are shown in panel B along with a two-exponential fit to the data.

RESULTS

Far-UV TRORD Experiments. In Figure 1A, the OMA TRORD spectra measured in the far-UV spectral region are represented by the pG_{446} spectrum and time-resolved spectra measured 10 ms and 2 s after initiation of the photocycle. The ORD signal collected at 10 ms shows an ~10% decrease in intensity (rotational strength) relative to the pG_{446} spectrum. Because the spectral changes in the ORD signal are small, only two time delays are shown.

Analysis of the OMA and the single-wavelength data best describes the dynamics of the PYP secondary structure with two exponential functions, 2 ± 0.8 and 650 ± 100 ms. The two-exponential fit is shown with the difference kinetic trace of the ORD data at all time delays in Figure 1B. Attempts to fit the far-UV data to three exponentials generated either

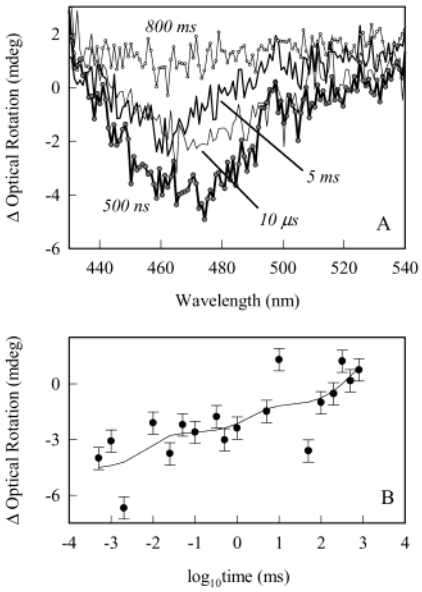

FIGURE 2: Visible TRORD data on the kinetics of the PYP photocycle. Four (500 ns, 10 μs, 5 ms, and 800 ms) of 19 spectra measured at different times are shown for the difference ORD data (A). A single-wavelength trace of all the difference ORD signals (472 nm) is shown with a three-exponential fit to the data in panel B.

a time constant faster than the time resolution of the experiment or two components with the same lifetime. The improvement of the residuals in going from a two-exponential to a three-exponential fit to the data is smaller than the noise.

Visible TRORD Experiments. In visible (chromophore) TRORD experiments, we focus only on the positive signal near 460 nm, although the signal of PYP also shows a negative ORD signal at ~380 nm. The negative OR band is extremely broad, with a full width at half-maximum of ~70 nm, and is difficult to measure on the TRORD apparatus because the wavelength dispersion of the detection system was limited to ~100 nm by the grating used in the spectrograph.

To clearly represent the visible TRORD data, only four of the 19 time-resolved difference OR spectra (500 ns, 10 μs, 5 ms, and 800 ms) that were collected are shown in Figure 2A. The difference ORD signal for the earliest measured time point, 500 ns, is negative with a minimum near 470 nm. At 10 μs, the intensity of the difference ORD signal is nearly half that of the signal at 500 ns, and at 800 ms, the ORD signal exhibits the full rotational strength of the pG_{446} state. The negative difference ORD signal at 5 ms shows a more pronounced decrease in magnitude at wavelengths greater than 470 nm than at wavelengths shorter than 470 nm. These changes in the visible TRORD data can be fit to three exponential processes with lifetimes of 10 ± 3 μs, 1.5 ± 0.5 ms, and 515 ± 110 ms. The three-exponential fit is shown with the kinetic trace of the TRORD data at all time points in Figure 2B.

TROD data in the visible region were measured and analyzed to demonstrate that the experimental conditions and results are consistent with those reported by previous TROD studies (*27*−*29*). Figure 3A shows the difference TROD spectra of PYP measured at 14, from a total of 30, time delays so that it is easier to follow the spectral changes. The

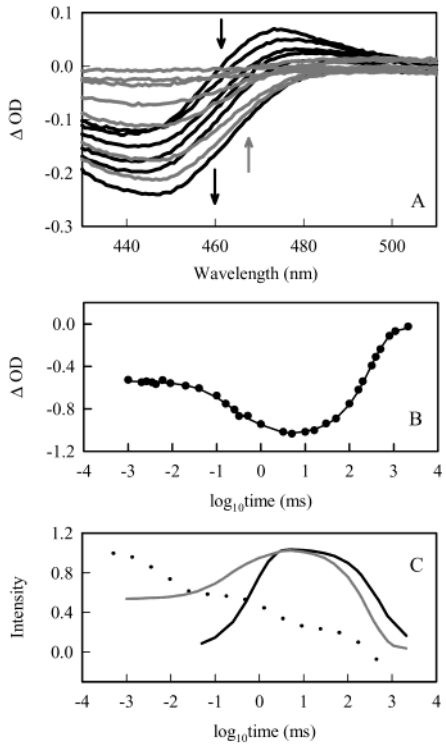

FIGURE 3: Comparison of the ORD and OD kinetics of the PYP photocycle probed in different spectral regions. (A) Difference TROD spectra measured at 14 (out of 30) time delays are shown. The spectra measured 1, 5, 100, 160, and 250 μs and 5 ms after initiation of the photocycle are shown in black, whereas the spectra obtained at 50, 100, 160, 400, and 500 ms and 1 and 2 s are shown in gray. In panel B, a single-wavelength trace (446 nm) of the TROD data is shown with the corresponding four-exponential fit. (C) The absolute value of the data from Figures 1B and 2B are normalized with respect to the absolute value of the intensity in panel B for easier comparison of the difference in kinetics measured with the far-UV ORD (black line), the visible OD (gray line), and visible ORD (dotted line) probes.

SVD and global analyses fit the TROD data to four exponential processes with lifetimes of 5 ± 1.5 μs, 145 ± 15 μs, 1.4 ± 0.6 ms, and 300 ± 20 ms. Three of the time constants (145 μs, 1.4 ms, and 300 ms) for this TROD study are consistent with those previously reported under similar sample conditions by Meyer et al. (272 μs, 2.8 ms, and 300 ms) (*27*) and Hoff et al. (250 μs, 1.2 ms, 150 ms, and 2 s) (*28*). In the kinetic studies by Meyer et al., the early (5 μs) and late (2 s) processes were not reported. This may be because data at a limited number of wavelengths around 440 nm were collected with a photomultiplier tube, which limits the spectral resolution of the measurements. The absence of a 5 μs process in the study by Hoff et al. (*28*) may be due to the time delays that were used in their experiments. Their multichannel absorbance spectra were measured from 10 to 25 ns and from 10 μs to 2 s, whereas their single-wavelength measurements used a gate of 10 μs. However, comparison of their difference absorption spectra at 25 ns and 10 μs shows changes that are similar to the 5 μs process reported here. A fifth exponential process with a time constant between 400 and 700 ms can be fit to our TROD data with a 3−8% improvement in the residuals. The inconsistency of this fifth exponential can be explained by the fact that our measurements did not focus on long times. Thus, with more measurements between 1 and 5 s, the fifth exponential

may approach the 2 s time constant reported by Hoff et al. (*28*).

Comparison of Kinetics of Secondary Structure and of Chromophore Signals. The absolute value of the single-wavelength traces from the difference far-UV (Figure 1B) and visible (Figure 2B) TRORD data are overlaid with that for the difference TROD signal at 446 nm (Figure 3B) in Figure 3C. During the formation of pB_{355}, the visible TRORD and TROD signals are considerably faster than the far-UV TRORD signal. However, the decay phase of the photocycle shows kinetics in the far-UV region that are similar to those in the visible region.

Secondary Structure Decomposition. CD spectra are used in this part of the study because they are more sensitive to differences in secondary structure than ORD signals. Recently, we have shown that the same exponential processes, regardless of the technique used to probe them (TRCD or TRORD spectroscopy), can describe the folding of cytochrome *c* in the reduced state. Thus, in this study of PYP kinetics, ORD detection is used primarily because it has a signal-to-noise advantage over CD (*46*), whereas equilibrium CD measurements help to support the structural interpretation of the ORD data.

Figure 4A shows a comparison of the ORD signals for the kinetically observed pB_{355} intermediate measured at 10 ms, the pB_{355} species present in photoequilibrium, and the acid-induced pB_{355} form (pB_{dark}, pH 1.5). The pB_{dark}, the equilibrium pB_{355}, and the kinetic pB_{355} ORD signals are 13, 11, and 10% smaller in magnitude, respectively, than the pG_{446} signal. In Figure 4A, the OR spectra are normalized at 230 nm to enhance any spectral differences in that band. The significant absorption of the probe light by the solvents, especially at low pH, limits the reliability of the data below 220 nm. Because the equilibrium OR spectra of pB_{dark} can be overlaid well with those of the equilibrium pB_{355} and pB_{355} measured at 10 ms, it is possible to make inferences about the secondary structure changes that occur in the kinetic form of pB_{355} by analyzing the equilibrium CD spectra of the pB_{dark} and pB_{355} species.

It might seem most reasonable to analyze the equilibrium CD spectrum of pB_{355} to understand the secondary structure changes that occur in pB_{355} at 10 ms since both species are induced by light. However, simultaneous illumination of the PYP sample and collection of the CD data result in light saturation of the detector. On the other hand, reliable CD data cannot be collected below 200 nm for pB_{dark} (pH 1.5) because of light absorption by the acid (Figure 4B). Because of these limitations, CD spectra were measured at various pH values from 8 to 3 to follow the secondary structure changes from pG_{446} to pB_{dark}, which is similar but not identical to pB_{355} (*50*). The secondary structure changes as a function of pH were analyzed by using the CDsstr program (*49*). In Figure 4B, the CD spectra for PYP at pH 8, 4, and 3 are shown with the respective reconstructed CD spectra that were generated by the CDsstr program. CD spectra for PYP at pH 6 were also collected and analyzed, but are not shown in the figure. The CD spectrum for pB_{dark} is shown, but could not be analyzed due to the unreliable signal below 200 nm.

The percentages of secondary structure reported by the CDsstr program are shown as a function of pH in Figure 4C. The results of the analysis are reported in terms of the

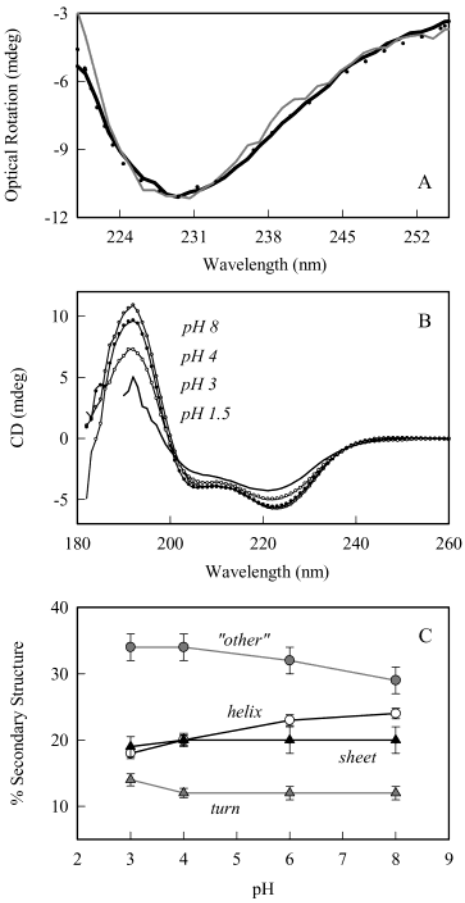

FIGURE 4: Analysis of the optical activity of PYP under different experimental conditions. In panel A, the ORD signals for pB_{355} (measured at 10 ms, black line), pB_{dark} (dotted line), and photoequilibrium pB_{355} (gray line) are normalized at 230 nm and overlaid to demonstrate the spectral similarity between the three species. This comparison is the basis for analysis of the secondary structure composition of the CD spectra for PYP. In panel B, the CD spectra for PYP measured at pH 8, 4, and 3 (circles) and 1.5 (black line, no circles) are shown. The reconstructed CD spectra (black lines) generated by the CDsstr program are shown along with the respective CD spectra at pH 8, 4, and 3. The percentages of secondary structures reported by the CDsstr analysis are shown as a function of pH in panel C. Data for each element of secondary structure are connected through a line so that the trends may be followed more easily.

percentages of α-helix, *β*-sheet, turn, and "other" structures, where "other" refers to random coil, to be consistent with the secondary structure reported by X-ray and NMR structural data. The contents of α-helix and *β*-sheet structures decrease from 24 to 18% and from 20 to 19%, respectively, upon titration of PYP from pH 8 to 3, and there is an increase from 29 to 34% and from 12 to 14% for the random coil and turn structures, respectively. The spectrum at pH 3, in contrast to the spectra at higher pH, is the only one that has a significant relative concentration of pB_{dark} (∼25%) (*37*, *51*). It is then likely that the secondary structure of pB_{dark} can be inferred by a fair interpolation of the data between pH 8 and 3: pB_{dark} has a significantly reduced α-helix content and an increased amount of random coil, as compared to pG_{446}.

DISCUSSION

The results of analyses with various time-resolved structure sensitive probes of the PYP photocycle have reported several

conformational changes that accompany formation and relaxation of the signaling state. These include (1) *trans*−*cis* isomerization of the chromophore on a sub-nanosecond time scale to form a red-shifted transient (pR, $\tau \sim 3$ ns, $\lambda_{max} = 465$ nm), (2) an intramolecular proton transfer to the anionic phenolic group of the chromophore to form a blue-shifted intermediate (pB′, $\tau \sim 250$ μs, $\lambda_{max} = 355$ nm), (3) partial exposure of the chromophore phenolic oxygen and large protein conformational changes (exposure of a large hydrophobic surface area) to accommodate the *cis* chromophore structure and to form the putative signaling state (pB, $\tau \sim 2$ ms, $\lambda_{max} = 355$ nm), and finally (4) deprotonation and *cis*−*trans* isomerization of the chromophore and protein refolding to re-form the initial PYP state (pG, $\tau \sim 500$ ms, $\lambda_{max} = 446$ nm).

By probing the changes in the ORD signal from the microsecond to seconds time scale, we have characterized the interaction of the chromophore with its protein environment (visible region) and the protein secondary structure (far-UV region) during the PYP photocycle from photoinitiation all the way through the recovery of the dark state. The optical activity in the 190−240 nm region is dominated by contributions from both the n−π* and the π−π* transitions of the protein backbone structure. In contrast, the origin of a protein chromophore ORD/CD visible spectrum, determined predominantly from studies of heme proteins, is due largely to the coupling of the asymmetrical electric dipoles of the chromophore with the allowed π−π* transitions of surrounding aromatic amino acid residues. However, it is also important to consider the inherent chirality of the chromophore and the distortion of the chromophore induced by the protein (*52*, *53*). Because ORD signals in different spectral regions report on different parts of the protein molecule, TRORD measurements will address the question of whether the chromophore and protein dynamics are sequential or synchronized.

Protein Structural Changes. The behavior of the TRORD changes in the far-UV region can be described by two exponential processes with lifetimes of 2 ± 0.8 and 650 ± 100 ms. The 2 ms component is correlated to partial unfolding of the PYP protein to form the pB_{355} intermediate, and the 650 ms process reflects the refolding of the protein in the last step of the photocycle. These assignments are consistent with the results from studies of heat capacity changes, $\Delta C_p^{\ddagger}$, during the PYP photocycle (*25*, *37*). The measured $\Delta C_p^{\ddagger}$ for re-formation of pG_{446} from pB_{355} indicates that this transition has the characteristics of a refolding process, whereas its numerical value is ∼30% of the value expected for complete unfolding of PYP (*25*). This suggests that ∼40 residues change conformation in the transition. The far-UV TRORD results also support the FTIR studies that associate a large conformational change with the formation of pB_{355} (*26*, *34*).

To assign the observed changes in the far-UV ORD signal to changes in secondary structure components, the optical activity of pB_{dark} was compared with that for pB_{355} (10 ms time point). Because the ORD signals for the β-sheet and α-helical conformations are nearly spectrally indiscriminate, with the ∼205 and 230 nm β-sheet signals only slightly shifted and broader than the α-helix signals at ∼198 and 233 nm (*54*−*58*), the changes observed in the TRORD data are interpreted by examining the pH-dependent changes in the equilibrium CD spectra during the acid-titrated formation of the pB_{dark} species. The CD spectrum for PYP at pH 1.5 (pB_{dark}) exhibits greater decreases in the rotational strengths at 208 and 222 nm than at 217 nm, which suggest that changes in the spectra can be attributed more to unfolding of α-helical than of β-sheet structure. These changes are verified by using the CDsstr algorithm to decompose the CD spectra measured at pH 8, 6, 4, and 3 into secondary structure components. Decomposition of these spectra (Figure 4B) suggests that the major changes in the secondary structure of the protein occur in the α-helical domains, with smaller changes taking place in the β-sheet segments. Because a calculation of complete unfolding of the N-terminal domain of PYP would lead to a decrease in helix content of ∼15%, taking into account the fact that the second α-helix in the crystal structure of PYP (α-2, residue numbers 20−23) (*21*) is relaxed into a poorly defined loop in solution (*23*), it is likely that a large part of the change in helical content is localized to the N-terminus. We are currently measuring the CD spectra of the dark and light-activated states of δ-25 PYP (trunc-PYP) where the N-terminus is truncated. Spectral decomposition of these CD data into secondary structure components will provide support for whether the changes in helical content suggested by these ORD/CD studies are indeed largely at the N-terminus. These results will be reported in a future publication.

The structural flexibility of the N-terminal segment and the changes of the photocycle kinetics in the absence of 6−27 amino acids of the N-terminus suggest an important functional role for this domain (*39*, *51*, *59*). The results of several structural probes of the photocycle of wild-type PYP (*60*) and the Met100Leu mutant (M100L) of PYP (*61*) suggest that the signaling state is less compact than the initial state. SAXS measurements on the M100L mutant report that there is a 16% increase in molecular volume upon formation of the blue-shifted, signaling intermediate (*61*). According to these authors, the expanded state, which shows a 40% decrease in α-helical content, may have a domain-localized protrusion of the protein that interacts with a receptor. An important role for the N-terminus, either in regulation of the photocycle kinetics or in receptor binding of the signaling state, would be consistent with the results obtained with plant phytochrome. The N-terminal segment of phytochrome has been proposed as a possible active site location (*62*, *63*) and changes its secondary structure also during the late stages of photoreceptor activation (*64*).

Chromophore Structural Changes. The behavior of the TRORD changes in the visible region can be described by three exponential decays with lifetimes of 10 ± 3 μs, 1.5 ± 0.5 ms, and 515 ± 110 ms. The visible ORD signal of pG_{446} has significant intensity, suggesting that the chromophore is in close contact with its neighboring amino acid residues. This is consistent with X-ray and NMR structural determinations that show the pG_{446} *trans* chromophore to be completely buried in the highly constraining, tightly packed major core of PYP (*21*, *23*). Within 500 ns of photoisomerization, the difference ORD signal is approximately half the magnitude of that for pG_{446}. Thus, the chromophore interaction with the surrounding aromatic amino acids is still significant at this time, although the negative intensity of this difference signal indicates that the distortion is in the opposite direction compared to that for the *trans* geometry. This result is

consistent with the observation of an early cryotrapped, pre-pR intermediate where the thioester linkage has rotated 166° relative to the plane formed by the aromatic ring of the chromophore (*8*). Although Genick et al. (*8*) report that the thioester oxygen stays in the rotated position for only a few nanoseconds, a time-resolved crystallographic molecular movie (1.8 Å) of the PYP photocycle from nanoseconds to seconds shows that the thioester oxygen is rotated from its original position from 1 ns until ~1 ms (*9*). The new environment of the flipped thioester oxygen is a hydrophobic cavity comprising aromatic amino acids Phe62, Phe75, Tyr94, Phe96, and the chromophore itself.

The presence of a distorted chromophore in this hydrophobic cavity at 500 ns is also supported by the far-UV TRORD data (Figure 1B), which show that the protein does not undergo significant global structural changes at times faster than 50 μs. This suggests that the *cis* chromophore "sees" a protein environment similar to that observed by the *trans* chromophore in pG_{446}. It is reasonable that the difference ORD signal at 500 ns reflects a chromophore−protein mismatch because the earliest significant structural change detected within the 500 ns time resolution of the TRORD experiments has a lifetime of 10 μs.

To understand the protein−chromophore relationship in the 10 μs process, the difference ORD signal observed at 10 μs is examined. When the 500 ns and 10 μs signals are normalized and overlaid, the difference observed at wavelengths greater than 490 nm is small enough that they are considered to have the same spectral shape. This suggests that the chromophore has structurally reoriented to partially relax its mismatched interaction with the aromatic amino acids of the proximal hydrophobic cavity. In support of this idea, time-resolved crystallographic studies (*9*) of the PYP photocycle show conformational changes correlated to the proximal side of the chromophore, where Ala67, Pro68, and Cys69 are part of a tight, S-shaped loop that is suggested to undergo a series of structural changes from tens of nanoseconds to tens of microseconds in response to the chromophore isomerization. Additionally, in the time range of 64 ns to 256 μs, overall protein structural changes are reportedly localized to the proximal (near Cys69) side of the chromophore.

Interestingly, the 10 μs component in the visible TRORD data has a counterpart in visible TROD data (5 μs decay time). This 5 μs TROD process (mainly a loss of positive absorption around 470 nm) has not been reported previously, but can be deduced from the data presented in the studies by Hoff et al. (*28*). The absence of a 10 μs process in the time-resolved FTIR data (*26*, *34*) may exist because the infrared studies focus on localized vibrations associated with the chromophore protonation state and the peptide backbone changes, whereas the changes in the visible ORD data monitor the global changes in the coupling of the chromophore with its protein environment. Detection of the early microsecond process in both TRORD and TROD not only identifies relaxation of the chromophore interaction with local aromatic residues in the hydrophobic cavity but also suggests changes in the chromophore coupling with nearby charged residues. This suggestion follows from the proposal that the absorption spectrum provides information about the proximity of charged amino acid residues to the chromophore. Specifically, it was shown that the absorption spectra of phytochrome and its photocycle intermediates are determined by the protonation state of the tetrapyrrole chromophore, as well as the interaction of the chromophore with the nearby charged amino acid residues (*65*).

The different sensitivities of absorption and optical activity methods explain why the chromophore protonation step (hundreds of microseconds) was detected in the TROD and not in the TRORD studies. To detect this process in TRORD measurements, the protonation of the chromophore must also influence a change in the surrounding amino acid residues. During the analysis of the visible TRORD data, a fourth process with a time constant of 100−200 μs could be fit to some of the data sets. Although this process was unstable and the residuals of a three-exponential fit showed no improvement with the addition of a fourth exponential, it suggests the possibility of a small process related to chromophore protonation. In addition, it follows that this process may be buried in the noise of the data and that protonation of the chromophore does not induce a large change in the chromophore chirality.

The difference signal at 5 ms is asymmetric, with less intensity at energies lower than ~470 nm, but can be overlaid with the difference ORD signal for pB_{355} generated by continuous illumination and pG_{446} at pH 8 (data not shown). This comparison indicates that the 1.5 ms process represents the chromophore changes associated with the formation of pB_{355}. According to X-ray crystallography studies, the pB_{355} intermediate is characterized by a *cis* chromophore where the phenolic oxygen is protonated and solvent-exposed. The sequence of these two events can be roughly mapped by protonation within hundreds of microseconds (*26*, *34*) and by movement of the chromophore that swings the guanidinium group of Arg52, which serves as the gateway to the hydrophobic chromophore cavity, into its fully open position after 1 ms (*9*). Because of the timing of the latter event and the 1.5 ms process observed in the TRORD data, the 1.5 ms component is attributed to the movement of the phenolic oxygen of the chromophore toward the solvent. This chromophore process is accompanied by the large global conformational changes in the protein secondary structure (τ = 2 ms) reported here and by time-resolved FTIR studies (*26*).

The difference signal at 800 ms shows no significant feature, indicating that the 515 ms component accounts for the re-formation of pG_{446} from pB_{355}. These TRORD results describe a photocycle mechanism where the chromophore and protein change synchronously in the inactivation process, but the signaling state is activated by a chromophore-mediated change in secondary structure. This mechanism is largely in agreement with the results of FTIR studies by Xie et al. (*26*) and partially in agreement with those by Brudler et al. (*34*). Because the visible TRORD data are noisy and limited in time points, further experiments are necessary to define the inactivation stage of the photocycle, as well as to determine if chromophore protonation effects a change in its chirality during signaling state activation. For the moment, the TRORD data suggest that the chromophore−protein interactions localized to the hydrophobic pocket are relaxed within 10 μs of initiation of the photocycle, and that this relaxation facilitates further changes in the chromophore (τ = 1.5 ms) that are coupled closely with secondary structure unfolding (τ = 2 ms).

ACKNOWLEDGMENT

We thank Drs. James W. Lewis, Robert A. Goldbeck, Istvan Szundi, Ronald Brudler, Keith Moffat, and Aihua Xie for valuable discussions.

REFERENCES

1. Sprenger, W. W., Hoff, W. D., Armitage, J. P., and Hellingwerf, K. J. (1993) *J. Bacteriol. 175*, 3096−3104.
2. Hoff, W. D., Devreese, B., Fokkens, R., Nugteren-Roodzant, I. M., van Beeumen, J., Nibbering, N., and Hellingwerf, K. J. (1996) *Biochemistry 35*, 1274−1281.
3. Hoff, W. D., Düx, P., Hård, K., Devreese, B., Nugteren-Roodzant, I. M., Crielaard, W., Boelens, R., Kaptein, R., van Beeumen, J., and Hellingwerf, K. J. (1994) *Biochemistry 33*, 13959−13962.
4. Baca, M., Borgstahl, G. E. O., Boissinot, M., Burke, P. M., Williams, D. R., Slater, K. A., and Getzoff, E. D. (1994) *Biochemistry 33*, 14369−14377.
5. van Beeumen, J. J., Devreese, B. V., van Bun, S. M., Hoff, W. D., Hellingwerf, K. J., Meyer, T. E., McRee, D. E., and Cusanovich, M. A. (1993) *Protein Sci. 2*, 1114−1125.
6. Kort, R., Vonk, H., Xu, X., Hoff, W. D., Crielaard, W., and Hellingwerf, K. J. (1996) *FEBS Lett. 382*, 73−78.
7. Perman, B., Šrajer, V., Ren, Z., Teng, T., Pradervand, C., Ursby, T., Bourgeois, D., Schotte, F., Wulff, M., Kort, R., Hellingwerf, K., and Moffat, K. (1998) *Science 279*, 1946−1950.
8. Genick, U. K., Soltis, S. M., Kuhn, P., Canestrelli, I. L., and Getzoff, E. D. (1998) *Nature 392*, 206−209.
9. Ren, Z., Perman, B., Šrajer, V., Teng, T.-Y., Pradervand, C., Bourgeois, D., Schotte, F., Ursby, T., Kort, R., Wulff, M., and Moffat, K. (2001) *Biochemistry 40*, 13788−13801.
10. Imamoto, Y., Shirahige, Y., Tokunaga, F., Kinoshita, T., Yoshihara, K., and Kataoka, M. (2001) *Biochemistry 40*, 8997−9004.
11. Gensch, T., Gradinaru, C. C., van Stokkum, I. H. M., Hendriks, J., Hellingwerf, K. J., and van Grondelle, R. (2002) *Chem. Phys. Lett. 356*, 347−354.
12. Hoff, W. D., Kwa, S. L. S., van Grondelle, R., and Hellingwerf, K. J. (1992) *Photochem. Photobiol. 56*, 529−539.
13. Imamoto, Y., Kataoka, M., and Tokunaga, F. (1996) *Biochemistry 35*, 14047−14053.
14. Baltuška, A., van Stokkum, I. H. M., Kroon, A., Monshouwer, R., Hellingwerf, K. J., and van Grondelle, R. (1997) *Chem. Phys. Lett. 270*, 263−266.
15. Ujj, L., Devanathan, S., Meyer, T. E., Cusanovich, M. A., Tollin, G., and Atkinson, G. H. (1998) *Biophys. J. 75*, 406−412.
16. Devanathan, S., Pacheco, A., Ujj, L., Cusanovich, M., Tollin, G., Lin, S., and Woodbury, N. (1999) *Biophys. J. 77*, 1017−1023.
17. Imamoto, Y., Kataoka, M., Tokunaga, F., Asahi, T., and Masuhara, H. (2001) *Biochemistry 40*, 6047−6052.
18. Chosrowjan, H., Mataga, N., Nakashima, N., Imamoto, Y., and Tokunaga, F. (1997) *Chem. Phys. Lett. 270*, 267−272.
19. Changenet, P., Zhang, H., van der Meer, M. J., Hellingwerf, K. J., and Glasbeek, M. (1998) *Chem. Phys. Lett. 282*, 276−282.
20. Mataga, N., Chosrowjan, H., Shibata, Y., Imamoto, Y., and Tokunaga, F. (2000) *J. Phys. Chem. B 104*, 5191−5199.
21. Borgstahl, G. E. O., Williams, D. R., and Getzoff, E. D. (1995) *Biochemistry 34*, 6278−6287.
22. Van Aalten, D. M. F., Crielaard, W., Hellingwerf, K. J., and Joshua-Tor, L. (2000) *Protein Sci. 9*, 64−72.
23. Düx, P., Rubinstenn, G., Vuister, G. W., Boelens, R., Mulder, F. A. A., Hård, K., Hoff, W. D., Kroon, A. R., Crielaard, W., Hellingwerf, K. J., and Kaptein, R. (1998) *Biochemistry 37*, 12689−12699.
24. Genick, U. K., Borgstahl, G. E. O., Ng, K., Ren, Z., Pradervand, C., Burke, P. M., Šrajer, V., Teng, T.-Y., Schildkamp, W., McRee, D. E., Moffat, K., and Getzoff, E. D. (1997) *Science 275*, 1471−1475.
25. Hoff, W. D., Xie, A., van Stokkum, I. H. M., Tang, X., Gural, J., Kroon, A. R., and Hellingwerf, K. J. (1999) *Biochemistry 38*, 1009−1017.
26. Xie, A., Kelemen, L., Hendriks, J., White, B. J., Hellingwerf, K. J., and Hoff, W. D. (2001) *Biochemistry 40*, 1510−1517.
27. Meyer, T. E., Yakali, E., Cusanovich, M. A., and Tollin, G. (1987) *Biochemistry 26*, 418−423.
28. Hoff, W. D., van Stokkum, I. H. M., van Ramesdonk, H. J., van Brederode, M. E., Brouwer, A. M., Fitch, J. C., Meyer, T. E., van Grondelle, R., and Hellingwerf, K. J. (1994) *Biophys. J. 67*, 1691−1705.
29. Meyer, T. E., Tollin, G., Hazzard, J. H., and Cusanovich, M. A. (1989) *Biophys. J. 56*, 559−564.
30. Meyer, T. E., Cusanovich, M. A., and Tollin, G. (1993) *Arch. Biochem. Biophys. 306*, 515−517.
31. Xie, A., Hoff, W. D., Kroon, A. R., and Hellingwerf, K. J. (1996) *Biochemistry 35*, 14671−14678.
32. Imamoto, Y., Mihara, K., Hisatomi, O., Kataoka, M., Tokunaga, F., Bojkova, N., and Yoshihara, K. (1997) *J. Biol. Chem. 272*, 12905−12908.
33. Hendriks, J., Hoff, W. D., Crielaard, W., and Hellingwerf, K. J. (1999) *J. Biol. Chem. 274*, 17655−17660.
34. Brudler, R., Rammelsberg, R., Woo, T. T., Getzoff, E. D., and Gerwert, K. (2001) *Nat. Struct. Biol. 8*, 265−270.
35. Borucki, B., Devanathan, S., Otto, H., Cusanovich, M. A., Tollin, G., and Heyn, M. P. (2002) *Biochemistry 41*, 10026−10037.
36. Salamon, Z., Meyer, T. E., and Tollin, G. (1995) *Biophys. J. 68*, 648−654.
37. van Brederode, M. E., Hoff, W. D., van Stokkum, I. H. M., Groot, M.-L., and Hellingwerf, K. J. (1996) *Biophys. J. 71*, 365−380.
38. Hendriks, J., Gensch, T., Hviid, L., van der Horst, M. A., Hellingwerf, K. J., and van Thor, J. J. (2002) *Biophys. J. 82*, 1632−1643.
39. Rubinstenn, G., Vuister, G. W., Mulder, F. A. A., Düx, P. E., Boelens, R., Hellingwerf, K. J., and Kaptein, R. (1998) *Nat. Struct. Biol. 5*, 568−570.
40. Yan, B., Nakanishi, K., and Spudich, J. L. (1991) *Proc. Natl. Acad. Sci. U.S.A. 88*, 9412−9416.
41. Rüdiger, W. (1992) *Photochem. Photobiol. 56*, 803−809.
42. Kort, R., Hoff, W. D., van West, M., Kroon, A. R., Hoffer, S. M., Vlieg, K. H., Crielaard, W., van Beeumen, J. J., and Hellingwerf, K. J. (1996) *EMBO J. 15*, 3209−3218.
43. Imamoto, Y., Ito, T., Kataoka, M., and Tokunaga, F. (1995) *FEBS Lett. 374*, 157−160.
44. Genick, U. K., Devanathan, S., Meyer, T. E., Canestrelli, I. L., Williams, E., Cusanovich, M. A., Tollin, G., and Getzoff, E. D. (1997) *Biochemistry 36*, 8−14.
45. Meyer, T. E. (1985) *Biochim. Biophys. Acta 806*, 175−183.
46. Shapiro, D. B., Goldbeck, R. A., Che, D., Esquerra, R. M., Paquette, S. J., and Kliger, D. S. (1995) *Biophys. J. 68*, 326−334.
47. Chen, E., Lapko, V. N., Lewis, J. W., Song, P.-S., and Kliger, D. S. (1996) *Biochemistry 35*, 843−850.
48. Chen, E., Lapko, V. N., Song, P.-S., and Kliger, D. S. (1997) *Biochemistry 36*, 4903−4908.
49. Johnson, W. C. (1999) *Proteins: Struct., Funct., Genet. 35*, 307−312.
50. Hoff, W. D., van Stokkum, I. H. M., Gural, J., and Hellingwerf, K. J. (1997) *Biochim. Biophys. Acta 1322*, 151−162.
51. van der Horst, M. A., van Stokkum, I. H., Crielaard, W., and Hellingwerf, K. J. (2001) *FEBS Lett. 497*, 26−30.
52. Blauer, G., Sreerama, N., and Woody, R. W. (1993) *Biochemistry 32*, 6674−6679.
53. Sreerama, N., and Woody, R. W. (2000) in *Circular Dichroism: Principles and Applications* (Berova, N., Nakanishi, K., and Woody, R. W., Eds.) 2nd ed., pp 601−620, John Wiley & Sons, New York.
54. Gratzer, W. B., and Cowburn, D. A. (1969) *Nature 222*, 426−431.
55. Blout, E. R., Schmier, I., and Simmons, N. S. (1962) *J. Am. Chem. Soc. 84*, 3193−3194.
56. Holzwarth, G., Gratzer, W. B., and Doty, P. (1962) *J. Am. Chem. Soc. 84*, 3194−3196.

57. Sarkar, P. K., and Doty, P. (1966) *Proc. Natl. Acad. Sci. U.S.A. 55*, 981−989.
58. Davidson, B., Tooney, N., and Fasman, G. D. (1966) *Biochem. Biophys. Res. Commun. 23*, 156−162.
59. Harigai, M., Yasuda, S., Imamoto, Y., Yoshihara, K., Tokunaga, F., and Kataoka, M. (2001) *J. Biochem. 130*, 51−56.
60. Lee, B.-C., Croonquist, P. A., Sosnick, T. R., and Hoff, W. D. (2001) *J. Biol. Chem. 276*, 20821−20823.
61. Sasaki, J., Kumauchi, M., Hamada, N., Oka, T., and Tokunaga, F. (2002) *Biochemistry 41*, 1915−1922.
62. Cherry, J. R., Hondred, D., Walker, J. M., and Vierstra, R. A. (1992) *Proc. Natl. Acad. Sci. U.S.A. 89*, 5039−5043.
63. Song, P.-S. (1994) *Spectrum 7*, 1−7.
64. Chen, E., Parker, W., Lewis, J. W., Song, P.-S., and Kliger, D. S. (1993) *J. Am. Chem. Soc. 115*, 9854−9855.
65. Björling, S. C., Zhang, C.-F., Farrens, D. L., Song, P.-S., and Kliger, D. S. (1992) *J. Am. Chem. Soc. 114*, 4581−4588.

BI020577O